J Mater Sci (2016) 51:9031–9042

Effect of alkaline excess on sintering, microstructural, and electrical properties of $Li_{0.12}Na_{0.88}NbO_3$ ceramics

Supratim Mitra[1,3,*], Pankaj K. Patro[2], and Ajit R. Kulkarni[1]

[1] *Department of Metallurgical Engineering and Materials Science, Indian Institute of Technology Bombay, Mumbai 400076, India*
[2] *Powder Metallurgy Division, Materials Group BARC, Vashi Complex, Navi, Mumbai, India*
[3] *Present address: NIIT University, Neemrana, Rajasthan 301705, India*

Received: 7 May 2016
Accepted: 20 June 2016
Published online: 29 June 2016

ABSTRACT

Sintering behavior in $Li_{0.12}Na_{0.88}NbO_3$ (LNN-12) ceramics has been investigated by analyzing the microstructures of the samples sintered at different temperatures (1050–1250 °C) and durations (1–6 h) to optimize the sintering conditions. An excess amount of Li_2CO_3 was added (1, 3, 5 mol%) to stoichiometric LNN-12 in order to compensate for the probable alkaline element loss at higher optimized sintering temperature. The addition of excess Li_2CO_3 into the starting materials and the effect of it on microstructure and electrical properties were investigated. Microstructural study of Li_2CO_3-added samples revealed abnormal grain growth, a characteristic feature of liquid phase sintering due to the low melting Li_2CO_3. The temperature and frequency dependence of dielectric constant shows two phase transitions in temperature dependence and low-frequency dispersion in the frequency dependence of dielectric plot. The observed frequency dispersion is attributed to dominant DC conductivity. The conduction mechanism was identified as diffusion of intrinsic Li^+ ion. The room-temperature dielectric constant and loss factor were found to increase with increase in Li_2CO_3 addition from 160 to 690 and 0.02 to 0.04, respectively. The electrical conductivity was found to increase two orders of magnitude (10^{-12}–10^{-10} Ω^{-1} cm^{-1}) in Li_2CO_3-added samples as compared to stoichiometric composition. The results obtained here give a strong evidence of the stoichiometry–microstructure and electrical properties correlation, thus emphasizing on the importance of processing parameters to tune the desired properties in $Li_{0.12}Na_{0.88}NbO_3$ ceramics.

Address correspondence to E-mail: supratimmitra2003@gmail.com

DOI 10.1007/s10853-016-0156-5

Introduction

Research in the domain of lead-free piezoelectric materials has progressively gained momentum due to environmental concerns of toxic lead (Pb). Lithium sodium niobate, $Na_{1-x}Li_xNbO_3$ (LNN), a promising lead-free piezoelectric system, has been receiving attention due to its potential in piezoelectric resonator and filter applications, for the compositions near the morphotropic phase boundary (MPB), viz., $x = 0.12$, commonly known as LNN-12 [1]. Both electromechanical coupling factor, k_p, and mechanical quality factor, Q_m, the figure of merit for these applications, found to be strongly dependent on the density and microstructure of the sintered sample [2, 3]. Hence, the knowledge of sintering behavior is essential in order to have good understanding of the final microstructure that evolves during sintering [4]. Usually, these alkali niobate-based ceramics are prepared by solid-state reaction (SSR) between alkaline carbonates and niobium pentoxide (Nb_2O_5) at temperature ~900 °C followed by sintering at temperature ~1250 °C. Synthesis of these niobates using conventional ceramic method leads to many unavoidable issues such as loss of alkali elements at elevated temperature that essentially create problems in achieving desired stoichiometry in the final product, chemical inhomogeneities, and abnormal grain growth. Sometimes, the variability of different decomposition/melting temperatures of starting materials leads to chemical inhomogeneities. The Nb_2O_5 starting material has a melting point of 1520 °C, whereas Na_2CO_3 and Li_2CO_3 have much lower melting points, 851 and 720 °C, respectively. Therefore, Nb_2O_5 is relatively refractory in nature, whereas Li_2CO_3 decomposes at a faster rate than Na_2CO_3 at lower temperature [5]. Another very important issue arises in synthesis process from the hygroscopic behavior of the alkaline carbonates, which are commonly used as raw materials for preparation by SSR [6, 7]. The humidity content in these raw materials headed toward a wrong weight measurements, if special care is not taken, and makes it difficult to maintain the proper stoichiometry in the final product. There are many techniques reported for sodium potassium niobate (KNN) system to minimize the effect of volatilization of alkali elements, for example spark plasma sintering [8] and double crucibles [9]. These methods are complicated, not cost-effective, and therefore undesirable for mass production in industries. Moreover, the use of excess alkali elements to compensate the loss was also conceived as an alternative [10]. However, it has been reported in the literature that excess alkali addition may promote grain growth, which deteriorates electrical properties in the resulting ceramics.

In view of the above, our strategy is to study the microstructure behavior of stoichiometric LNN-12 ceramics and also the effect of introducing excess Li_2CO_3 into starting mixture in order to compensate possible alkali element losses during sintering at higher temperature. Particle size and morphology are also investigated to better understand the densification behavior. Here, we have investigated the effect of only Li_2CO_3 addition on microstructure and electrical conductivity as it is well known that the tendency of Li loss is more pronounced than Na [11, 12].

Materials and methods

All the samples in this study were prepared using conventional solid-state reaction followed by sintering. The starting raw materials were reagent-grade Nb_2O_5, Na_2CO_3 (both 99.5 % pure, Loba Chemie, India), and Li_2CO_3 (99.0 % pure, Merck, India) and were kept in electrical oven for overnight at 150 °C to avoid the humidity content in alkali carbonates. These were mixed in the desired stoichiometry of $Na_{1-x}Li_xNbO_3$ ($x = 0.12$) for one sample, and deliberately excess Li_2CO_3 of 1, 3, 5 mol% was added with stoichiometric $Li_{0.12}Na_{0.88}NbO_3$ to prepare the other samples. The mixtures were ball-milled for 24 h in alcohol to obtain proper mixing and a surface-active fine powder. The finely mixed constituent powders were then solid-state-reacted at 900 °C for 5 h to get phase pure powder. The size distribution of the phase pure powder was measured using laser diffraction particle size analyzer (Beckman Coulter, LS 13 320). The powders were then uniaxially pressed at 150 MPa into pellets. To obtain the optimized sintering condition, the stoichiometric LNN-12 green pellets were sintered at different temperatures (1050–1250 °C) for varied durations (1, 2, 4, and 6 h) in air. The phase purity of the stoichiometric LNN-12 and excess Li_2CO_3-added samples was checked by powder X-ray diffraction (XRD) at room temperature using X-ray diffractometer (X'Pert, PANalytical) with Cu-Kα radiation. For this, the final sintered pellets were finely crushed and annealed at 500 °C for 12 h

to reduce residual stress. The microstructural analysis of polished and thermally etched sintered pellets was carried out using scanning electron microscope (SEM) (JEOL-JSM 7600F). The average grain size, G, was estimated using a linear intercept method for the data collected over 200–300 grains, sampled at different locations of each of the SEM micrographs, using a standard image analysis software (ImageJ, NIH, USA). The dielectric constant and electrical conductivity of the samples were recorded using Impedance Analyzer (Alpha High Resolution, Novocontrol) in the frequency range 0.1–10^6 Hz over the temperatures 50–500 °C.

Results and discussion

Phase analysis

Figure 1 shows XRD pattern of stoichiometric LNN-12 and excess Li_2CO_3 (1, 3, 5 mol%)-added samples. Within the detectable limit of XRD, stoichiometric LNN-12 and compositions with 1 and 3 mol% Li_2CO_3-added samples show a characteristics pure perovskite structure. The peaks in the XRD pattern are indexed to a major orthorhombic phase (JCPDS# 033-1270) and is characterized by splitting of (202)/(080) peaks. However, in addition to pure perovskite phase, for $x = 5$ mol% Li_2CO_3-added sample, a minute secondary phase was detected (indicated as * in Fig. 1). This phase could be assigned to Li_3NbO_4 with a cubic structure (JCPDS# 016-0459) which is possibly a low melting liquid phase and thus contributes to abnormal grain growth. The lattice parameters and the unit cell volumes for all the compositions are too calculated and are listed in Table 1.

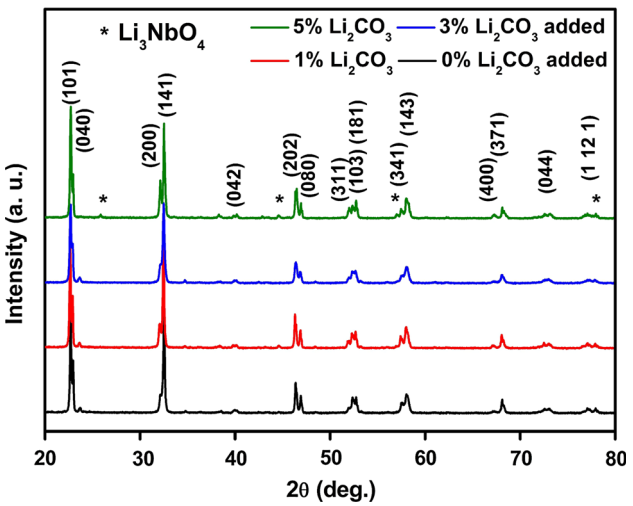

Figure 1 XRD patterns of stoichiometric LNN-12 and 1, 3, 5 mol% Li_2CO_3-added LNN-12 samples. Minor secondary phase Li_3NbO_4 is marked as (*asterisks*) in excess Li_2CO_3-added samples.

Particle morphology and size distribution

The SEM micrographs of calcined (SSR) powder of stoichiometric LNN-12 and excess Li_2CO_3 (1, 3, 5 mol%)-added samples are shown in Fig. 2. In order to confirm the particle size distribution (PSD) that obtained from SEM data, as shown in inset of Fig. 2a–d, the particle size analysis of the calcined powder was also carried out using laser diffraction particle size analyzer, and their distributions are shown in Fig. 2e. For stoichiometric LNN-12, a uniform and narrow particle size distribution has been observed with an average particle size ~0.5 μm; however, Li_2CO_3-added samples show a non-uniform and broadened distribution with slightly higher average particle size (>0.5 μm). The non-uniformity exists in the particle size distribution in Li_2CO_3-added samples as few coarser particles could be due to secondary crystallization where coarser particles are formed coalescing smaller particles. The observed coarser particles act as nucleation centers for grain growth during sintering [10].

Microstructural development in stoichiometric sample

The SEM images of polished and thermally etched surfaces of the LNN-12 discs, sintered at different

Table 1 Variation in lattice parameters and unit cell volume of stoichiometric LNN-12 and 1, 3, 5 mol% Li_2CO_3-added LNN-12 samples

Addition of excess Li_2CO_3 (%)	a (Å)	b (Å)	c (Å)	V (Å^3)
0	5.5000	5.5658	15.4792	473.84
1	5.4962	5.5699	15.4751	473.74
3	5.4957	5.5605	15.4879	473.29
5	5.4948	5.5690	15.4743	473.44

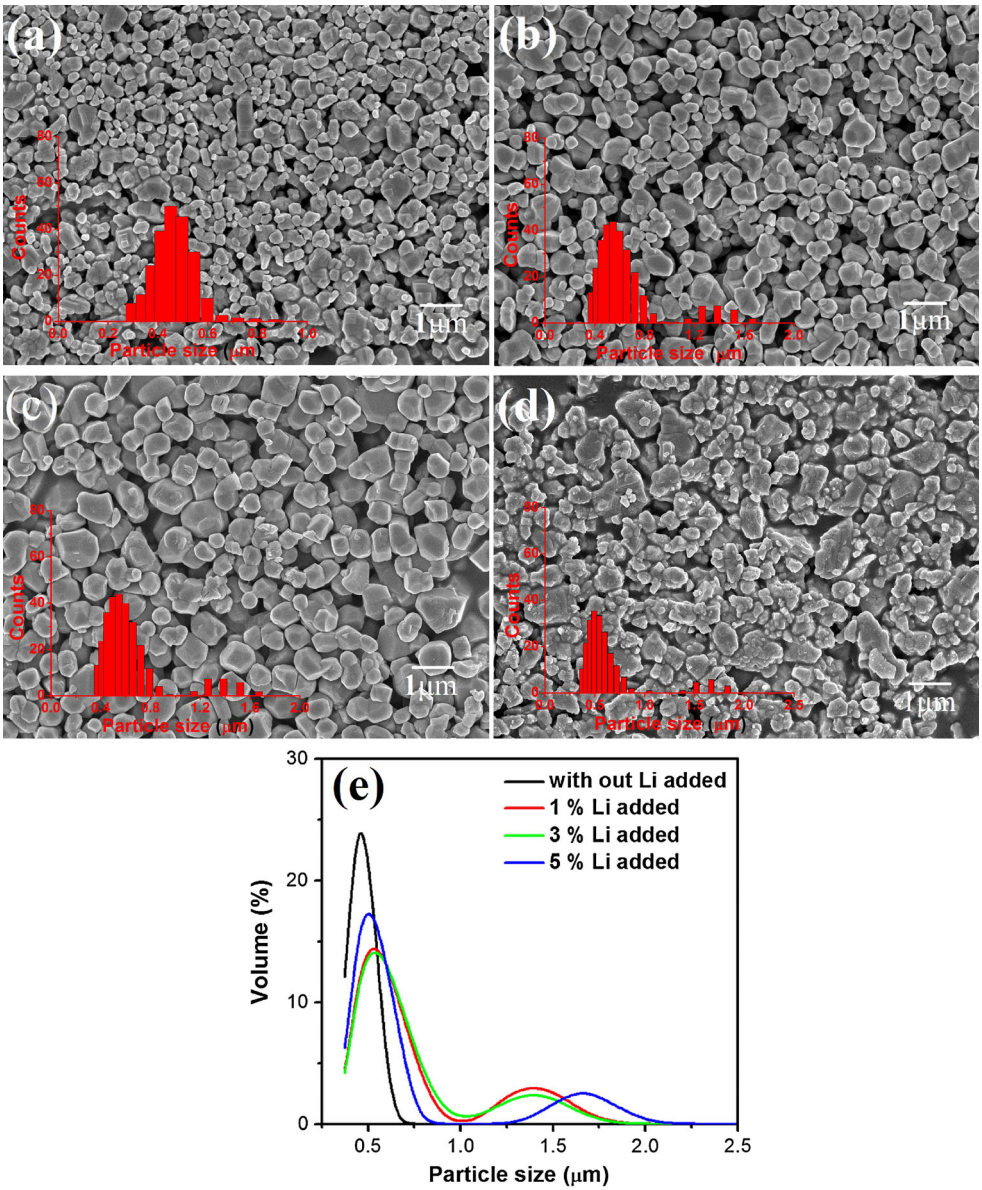

Figure 2 **a**–**d** SEM micrographs of calcined (SSR) powder, and **e** particle size distribution of stoichiometric LNN-12 and excess Li_2CO_3 (1, 3, 5 mol%)-added samples measured using laser diffraction particle size analyzer.

temperatures (1050–1250 °C) with a dwelling duration of 2 h, are shown in Fig. 3. For all the samples, uniform and well-developed grains with no exaggerated grain growth are seen. The average grain size and relative density obtained from these samples are compiled in Table 2. The graphs in Fig. 4a show the sintering temperature-dependent densification and grain growth in the LNN-12 compacts. In the temperature range 1050–1190 °C, the sintered density increases from 90.5 to 95.9 % and the average grain size from 1.1 to 2.3 μm (Fig. 4a). The densification process, as expected, has proceeded through progressive elimination of the connected open porosity, and is primarily via the lattice and the grain boundary diffusion paths [13]. At higher sintering temperatures ($T > 1190$ °C), though further densification is marginal, an accelerated grain growth is clearly seen (Fig. 4b). Reverting to Fig. 3 and Table 2, as the temperature is progressively increased from 1190 to 1220 °C, and finally to 1250 °C, the grain size has also increased from 2.3 (Fig. 3d) to 3.1 μm (Fig. 3e) to 4.2 μm (Fig. 1f). The relative increase in grain size is substantial, whereas only a nominal increase from 95.9 to 96.8 % (Fig. 2a) is seen in the overall sintered density. A careful observation of the grain size distribution histograms, given as insets in Fig. 3d–f, clearly shows that the smaller grains, in spite of not having many curved boundaries, are

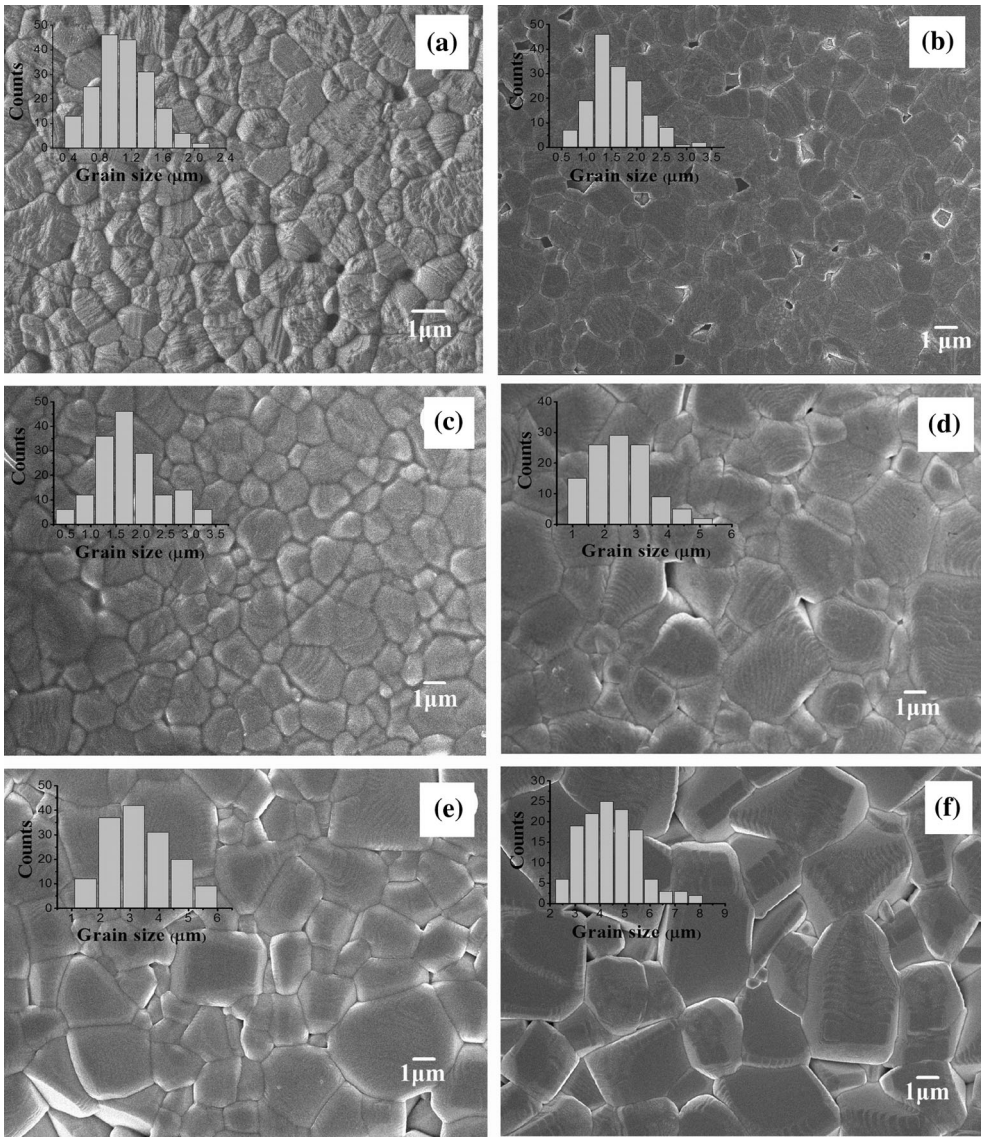

Figure 3 SEM photomicrographs of the polished and thermally etched LNN-12 pellets sintered at **a** 1050 °C/2 h, **b** 1100 °C/2 h, **c** 1150 °C/2 h, **d** 1190 °C/2 h, **e** 1220 °C/2 h, and **f** 1250 °C/2 h, showing clean phase and progressively improved densification and grain size.

Table 2 Variation in the average grain size and relative density (%) of the LNN-12 ceramic samples sintered at different temperatures (1050–1250 °C) for 2 h

Temperature (°C)	Relative density (% ρ_{th})	Average grain size (μm)
1050	90.5	1.1
1100	92.5	1.5
1150	95.6	1.6
1190	95.9	2.3
1220	96.1	3.1
1250	96.8	4.2

progressively merged into the larger grains. This is akin to Oswald ripening. Additionally, the residual dispersed open porosity in the low-temperature (≤1190 °C)-sintered sample indicates insufficient sintering parameters (time and temperature). It is well known that definite activation energy is required

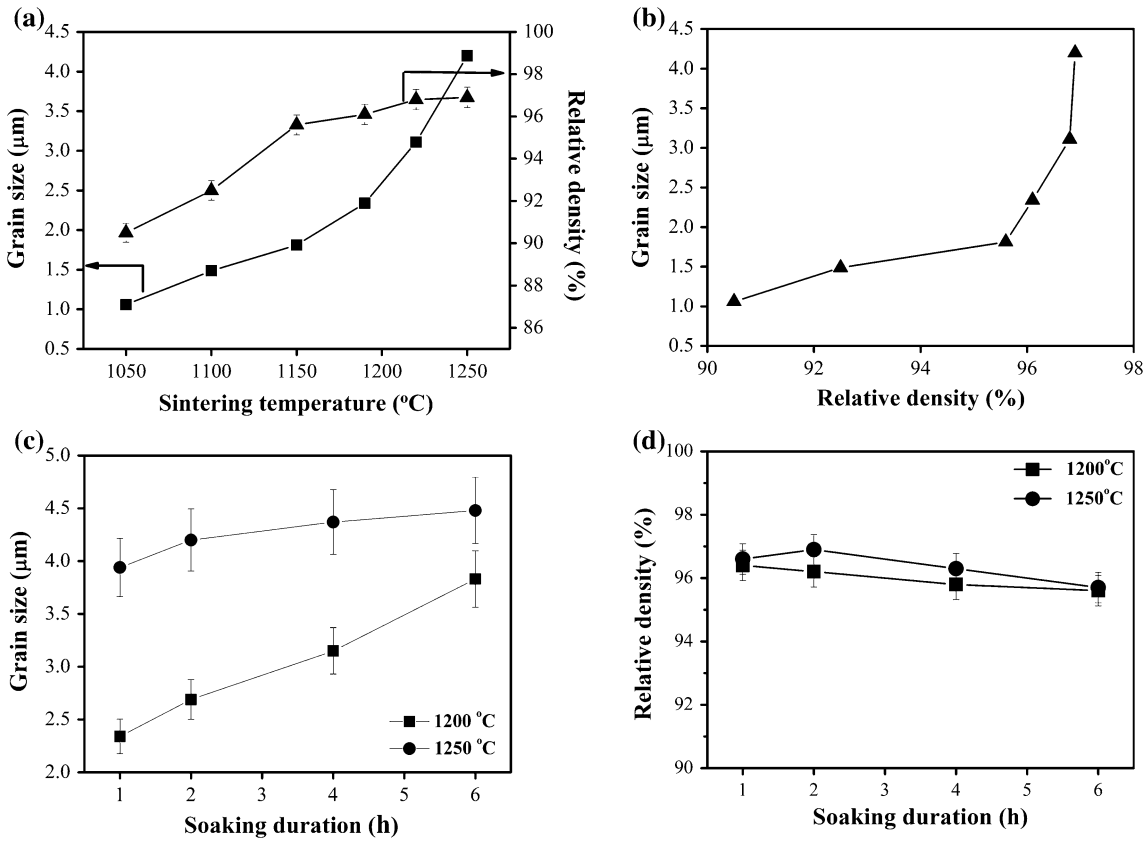

Figure 4 Variation in **a** grain size and relative density (%) with sintering temperatures (1050–1250 °C), **b** grain size with relative density (%) that obtained from (**a**). Variation in **c** grain size and **d** relative density (%) with different soaking durations (1–6 h) for LNN-12 ceramic sintered at 1200 and 1250 °C.

for the grain boundary movement, and if either the temperature or time is insufficient, it leads to discrete open pores. At higher sintering temperatures (≥1190 and ≤1250 °C), the open pores collapse resulting in a relative decrease in numbers of pores and an accelerated grain growth [14].

In the stoichiometric LNN-12 ceramic pellets, it is seen that at $T > 1190$ °C, the grain growth proceeds at a faster rate compared to the rate of densification. In order to distinguish the difference in the rate of grain growth between the earlier and the later stages of sintering, the samples have been systematically subjected to isothermal sintering at two different temperatures, viz., 1200 °C (a little higher than 1190 °C) and 1250 °C, and for dwelling durations of 1, 2, 4, and 6 h. The average grain size variation with soaking duration, for 1200 and 1250 °C, is shown in Fig. 4c and also listed in Table 3. The average grain size in the samples sintered at 1200 °C has increased from 2.3 to 3.8 μm for the samples sintered at 1250 °C increased marginally from 3.9 to 4.5 μm, while the soaking duration has been increased from 1 to 6 h. This indicates that at the early stage of sintering, the rate of grain growth is higher, which is primarily led by grain boundary diffusion. However, this progressively slows down with soaking time and reaches a minimum at the final grain size, at the specified sintering temperature. Figure 4d shows the variation in sintered density with soaking durations for the samples sintered at 1200 and 1250 °C. A highest value of sintered density of 96.9 % was obtained for the samples sintered at 1250 °C for 2 h. A decrease in density for soaking duration higher than 2 h has been observed for all samples which may be attributed to loss of alkali elements at elevated temperature and long soaking durations. An optimized sintering condition therefore has been decided on the basis of highest measured sintered density (96.9 %) and moderate grain size (4.2 μm) and found to be 1250 °C for 2 h.

Table 3 Variation in average grain size with soaking durations for isothermal sintering at 1200 and 1250 °C of LNN-12 ceramic

Temperature (°C)	Soaking duration (h)	Average grain size (μm)
1200	1	2.3
	2	2.7
	4	3.2
	6	3.8
1250	1	3.9
	2	4.2
	4	4.4
	6	4.5

Microstructural development in excess Li_2CO_3-added samples

Figure 5a–c shows the SEM images of polished and thermally etched surfaces of the stoichiometric LNN-12 and excess Li_2CO_3 (1, 3 mol%)-added pellets, sintered at the same optimized sintering condition (1250 °C for 2 h) for the sake of comparing. The 5 mol% Li_2CO_3-added sample did not sustain the sintering temperature of 1250 °C and melted. This has been further substantiated by differential scanning calorimetry (DSC) experiments carried out at a heating rate of 10 °C/min for stoichiometric LNN-12 and excess Li_2CO_3 (1, 3, 5 mol%)-added powder samples as indicated in Fig. 6. From the inset of Fig. 6, it can be seen that there is no endothermic peak for stoichiometric LNN-12 and 1–3 mol% Li_2CO_3-added samples, while a weak peak ~1135 °C for 5 mol% Li_2CO_3-added sample has been observed. This confirms the melting of the 5 mol% Li_2CO_3-added sample and therefore not considered for further investigation. The effect of excess Li_2CO_3 addition has a significant effect on the microstructure development as shown in Fig. 5. For stoichiometric

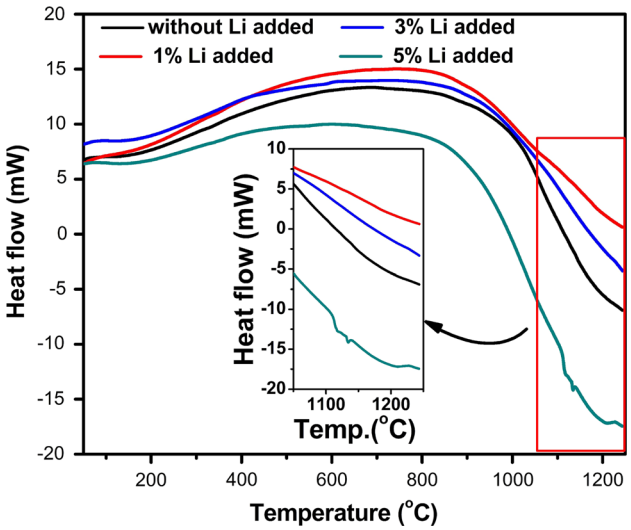

Figure 6 DSC curves for stoichiometric LNN-12, along with excess Li_2CO_3 (1, 3, 5 mol%)-added powder samples.

LNN-12 sample, a uniform and normal grain growth with an average grain size of 4.2 μm (as discussed in "Particle morphology and size distribution" section) is observed as shown in Fig. 5a. However, for Li_2CO_3-added sample, grain size distributions are no

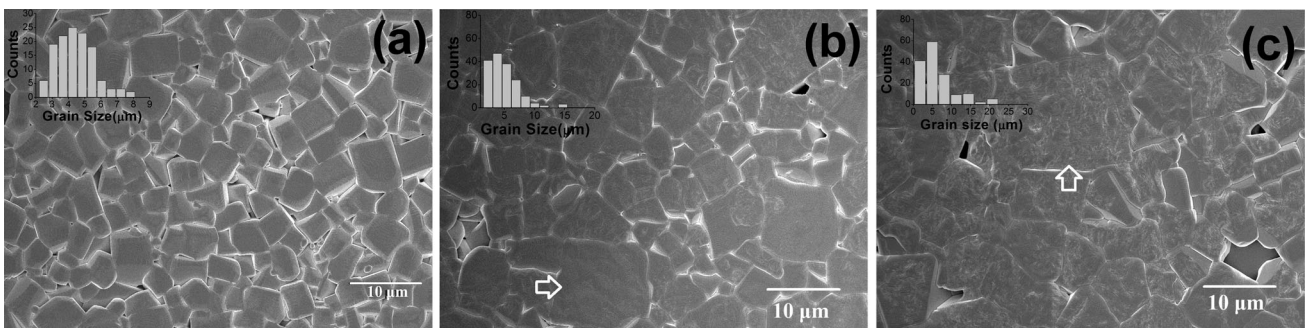

Figure 5 SEM photomicrographs of the polished and thermally etched pellets sintered at 1250 °C/2 h. **a** Stoichiometric LNN-12, **b** 1 mol% Li_2CO_3-added, and **c** 3 mol% Li_2CO_3-added samples.

longer uniform, but consist of a large number of small grains and a small fraction of large size grains as shown in the inset of the grain size distribution histogram in Fig. 5b, c. For 1 mol% excess Li_2CO_3-added sample, the average grain size remains same (~4.2 μm); however, larger grains reach size up to 15 μm as marked by the arrow in Fig. 5b. Further, in 3 mol% Li_2CO_3-added sample, the average grain size increases from 4.2 to 4.9 μm, while larger grains of size ~23 μm (inset of Fig. 5c) have been observed. These signify that addition of excess Li_2CO_3 promotes an abnormal grain growth (AGG). The observation of AGG is believed to originate from the formation of low melting liquid phase at the non-stoichiometric (Li-rich/Na-poor) grain boundaries, which enhances dramatically the atomic mobility and resulting in AGG [15, 16].

Electrical properties

Temperature-dependent permittivity in the range 50–500 °C measured at selected frequencies is depicted in Fig. 7. Both the real (ε') and imaginary (ε'') parts of permittivity show two peaks, representing a ferroelectric to paraelectric transition at T_m and ferroelectric to ferroelectric transition at T_{ff} which appears at the lower temperature side of permittivity maxima. Broadening of the permittivity peaks in ε' (T) are observed near both the transition temperatures (T_m, T_{ff}); however, frequency-dependent dispersion in T_m has not been observed. This could be related to diffuse ferroelectric phase transition observed in pure LNN system [11] nevertheless of different characteristics of classical relaxor ferroelectrics. The usual ground for the appearance of

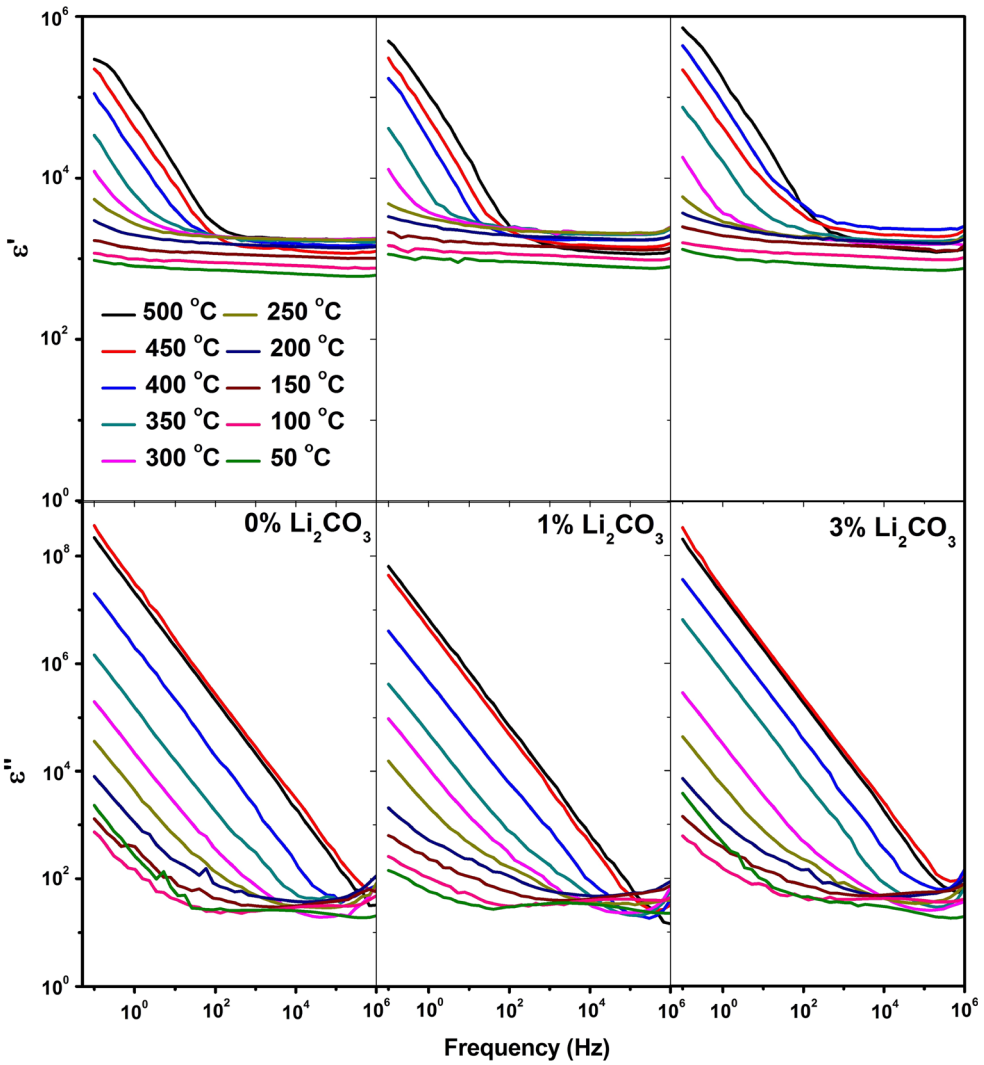

Figure 7 Frequency dependence (10^{-1}–10^6 Hz) of real (ε') and imaginary (ε'') parts of permittivity measured at different temperatures (50–500 °C with step of 50 °C) for stoichiometric LNN-12 (0 mol%) and excess Li_2CO_3 (1, 3 mol%)-added samples.

diffuse phase transition is structural frustration induced due to an equivalent site in the lattice that is occupied by different types of cations. In accession, in the present study, both the transition peaks (T_m, T_{ff}) are set up in very close proximity, which also contribute to a diffuse phase transition. In stoichiometric LNN-12 and 1 % Li_2CO_3-added sample, position of transition peaks is almost at the same temperatures, T_m = 325, 316 °C and T_{ff} = 217, 220 °C, respectively. This is in agreement with the minute change in unit cell volume as listed in Table 1. However, well-separated peaks at T_m = 420 °C and T_{ff} = 195 °C for 3 % Li_2CO_3-added sample were observed. The frequency dependence (0.01–1 MHz) of real and imaginary parts of dielectric permittivity (ε' and ε'', respectively) on a log–log scale in the temperature range 50–500 °C (with step of 50 °C) is depicted in Fig. 8. Both the parameters (ε' and ε'', respectively) show strong low-frequency dispersion in dielectric permittivity (LFDD), characteristic of the high-temperature region due to a dominant DC conduction process. The electrical conductivity in Li_2CO_3-added non-stoichiometric LNN-12 might be associated with defects and their migration [17]. In stoichiometric LNN-12, the conduction is mainly electronic as the intrinsic lithium-ion (Li^+) concentration is small compared to electronic contribution, whereas that in the non-stoichiometric material is ionic [18]. Samples with excess Li_2CO_3 added, diffusion of Li^+ enhances greatly which results in higher electrical conductivity.

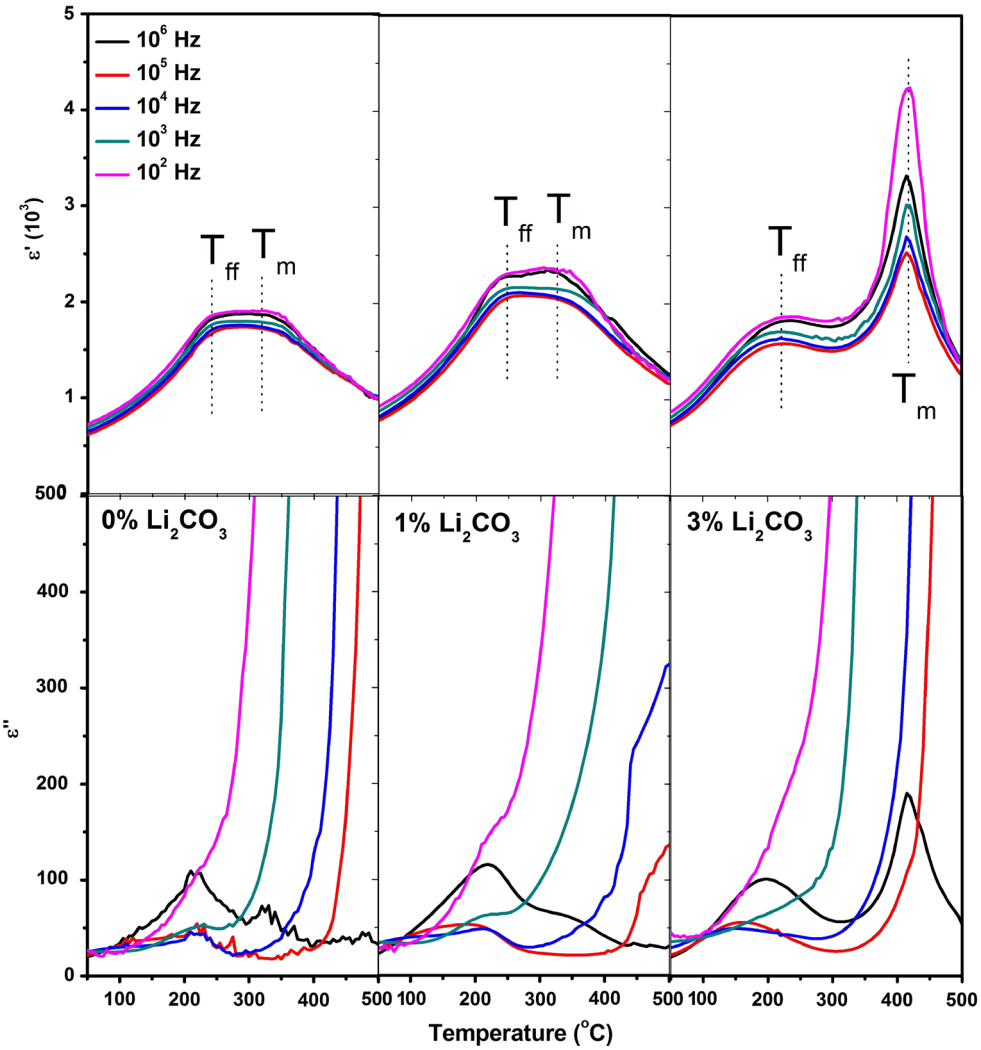

Figure 8 Temperature dependence (50–500 °C) of real (ε') and imaginary (ε'') parts of permittivity measured at different frequencies (10^2–10^6 Hz) for stoichiometric LNN-12 (0 mol%) and excess Li_2CO_3 (1, 3 mol%)-added samples.

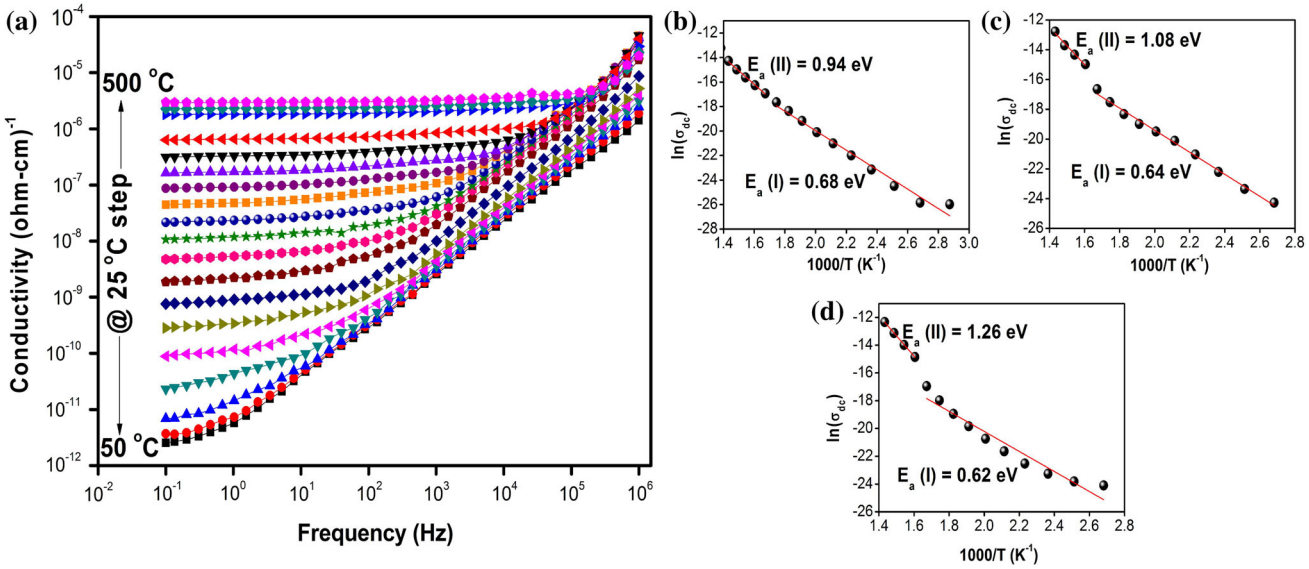

Figure 9 **a** Representative graph for frequency-dependent electrical conductivity at various temperatures for stoichiometric LNN-12, **b**–**d** plot of ln σ_{dc} versus 1000/T for stoichiometric LNN-12 and 1, 3 mol% Li_2CO_3-added samples, respectively. Activation energies are obtained from the linear fit.

So, to look into the conductivity behavior in Li_2CO_3-added LNN-12, temperature and frequency dependence of electrical conductivity was studied. The temperature-dependent DC conductivity response of stoichiometric LNN-12 and Li_2CO_3-added samples is presented in Fig. 9b–d. The data represent the Arrhenius relation $\sigma_{dc} = \sigma_0 \exp(-E_a/kT)$, where σ_0 is a pre-exponential factor and E_a, k, and T represent the activation energy for conduction, Boltzmann's constant, and the absolute temperature, respectively. The activation energy for conduction (E_a) was estimated by the slope of the ln σ versus 1000/T plot. The DC conductivity was determined from the total conductivity following Jonscher's power law: $\sigma_{total} = \sigma_{dc} + A\omega^n$, where second part of the equation is associated with the frequency-dependent conductivity [19]. The representative graph of frequency-dependent total electrical conductivity at various temperatures for the stoichiometric LNN-12 sample is presented in Fig. 9a. For all the samples, two different regions of conductivity have been observed mentioned as region I and region II associated with ferroelectric and paraelectric phase, respectively, as shown in Fig. 9b–d. In the low-temperature region I (ferroelectric phase), extrinsic conduction resulting from impurity ions present in the lattice dominates, whereas intrinsic ionic conduction resulting from the movement of the component ions occurs in the high-temperature paraelectric phase [20, 21]. In stoichiometric LNN-12 with no excess Li^+, the dominating conduction is mainly electronic and shows activation energy of 0.68 eV in the low-temperature region. With the increase in Li^+ concentration, a deviation from stoichiometry occurs and conduction mechanism changes to ionic. At higher temperature, the values of activation energy obtained ($\sim$1 eV) are normally associated with thermally driven intrinsic ionic conduction for stoichiometric LNN-12 and extrinsic ionic conduction for non-stoichiometric LNN-12 due to mobility of Li^+ [17, 22].

In a comparative study, the variation in dielectric constant, loss factor, and electrical conductivity with measuring frequency at room temperature is shown in Fig. 10. The room-temperature parameter values at 1 kHz such as dielectric constant are found to increase from 160 to 475 °C, as Li_2CO_3 is increased from stoichiometric to 1 % and from 160 to 690 °C for 3 % Li_2CO_3-added sample (Fig. 10a). The loss factor has increased from 0.02 to 0.03 for stoichiometric to 1 % and finally reaches 0.04 for 3 % Li_2CO_3-added sample (Fig. 10b). The electrical conductivity value for stoichiometric LNN-12 is found to be $\sim 10^{-12}$ $(\Omega\ cm)^{-1}$ and increases up to two orders of magnitude for 3 % Li_2CO_3-added sample (Fig. 10c), which is found the more influential effect of excess Li_2CO_3 addition.

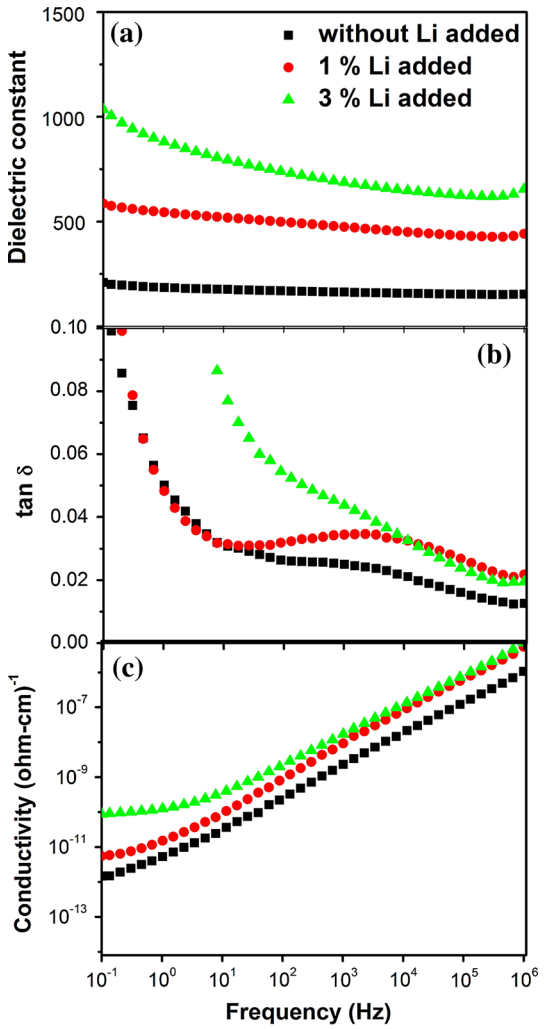

Figure 10 Frequency dependence of **a** dielectric constant, **b** loss factor, and **c** electrical conductivity of stoichiometric LNN-12 and 1, 3 mol% Li_2CO_3-added LNN-12 samples measured at room temperature.

Conclusions

The microstructural development of stoichiometric LNN-12 has been investigated systematically, and optimized sintering condition has been obtained on the basis of highest achieved density with moderate grain size. Excess Li_2CO_3 has been added to compensate possible alkali evaporation during sintering at elevated temperature. An abnormal grain growth has been observed for higher Li_2CO_3-added sample, and it is concluded that addition of excess Li_2CO_3 in starting material should be restricted up to 3 mol%. The room-temperature electrical conductivity has been found to be two orders of magnitude higher than that of stoichiometric LNN-12 because of the uncompensated excess Li_2CO_3 in the lattice. The room-temperature dielectric constant increases almost 4.5 times (160–690), whereas a change in loss factor from 0.02 to 0.04 has been observed when excess Li_2CO_3 is added up to 3 mol%. Therefore, it can be understood from the results that there is a marked effect of Li_2CO_3 addition on microstructure and dielectric properties. Hence, for a specific application, it is important to maintain proper stoichiometry in ceramics for microstructure and the development of appropriate processing schedule to optimize its electrical properties.

Acknowledgements

S.M. would like to thank SAIF, IIT, Bombay, for providing SEM facility.

Compliance with ethical standards

Conflict of interest All the authors certify that they have no affiliations or involvement in any organization or entity with any financial interest or non-financial interest in the subject matter or materials discussed in this manuscript.

References

[1] Henson RM, Zeyfang RR, Kiehl KV (1977) Dielectric and electromechanical properties of (Li, Na)NbO_3 ceramics. J Am Ceram Soc 60:15–17

[2] Hardiman B, Henson RM, Reeves CP, Zeyfang RR (1976) Hot pressing of sodium lithium niobate ceramics with perovskite-type structures. Ferroelectrics 12:157–159

[3] Chen Q, Peng Z, Liu H, Xiao D, Zhu J, Zhu J (2010) The crystalline structure and phase-transitional behavior of $(Li_{0.12}Na_{0.88})(Nb_{1-x\%}Sb_{x\%})O_3$ lead-free piezoelectric ceramics with high Q_m. J Am Ceram Soc 93:2788–2794

[4] Mitra S, Kulkarni AR, Prakash O (2013) Densification behaviour and two stage master sintering curve in lithium sodium niobate ceramics. Ceram Int 39:S65–S68

[5] Pelton AD, Bale CW, Lin PL (1984) Calculation of phase diagrams and thermodynamic properties of 14 additive and reciprocal ternary systems containing Li_2CO_3, Na_2CO_3, K_2CO_3, Li_2SO_4, Na_2SO_4, K_2SO_4, LiOH, NaOH, and KOH. Can J Chem 62:457–474

[6] Maeder MD, Damjanovic D, Setter N (2004) Lead free ferroelectric materials. J Electroceram 13:385–392

[7] Jenko D, Malic B, Bernard JB, Cilensek J, Kosec M (2003) Synthesis and sintering of KNN 50/50 ceramics. Mater Technol 37:22–28

[8] Li J-F, Wang K, Zhang B-P, Zhang L-M (2006) Ferroelectric and piezoelectric properties of fine-grained $Na_{0.5}K_{0.5}NbO_3$ lead-free piezoelectric ceramics prepared by spark plasma sintering. J Am Ceram Soc 89:706–709

[9] Zhen Y, Li J-F (2006) Normal sintering of (K, Na)NbO_3-based ceramics: influence of sintering temperature on densification, microstructure, and electrical properties. J Am Ceram Soc 89:3669–3675

[10] Bomlai P, Wichianrat P, Muensit S, Milne SJ (2007) Effect of calcination conditions and excess alkali carbonate on the phase formation and particle morphology of $Na_{0.5}K_{0.5}NbO_3$ powders. J Am Ceram Soc 90:1650–1655

[11] Mitra S, Kulkarni AR, Prakash O (2013) Diffuse phase transition and electrical properties of lead-free piezoelectric $(Li_xNa_{1-x})NbO_3$ $(0.04 \leq x \leq 0.20)$ ceramics near morphotropic phase boundary. J Appl Phys 114:064106

[12] Cheng L-Q, Wang K, Yao F-Z, Zhu F, Li J-F (2013) Composition inhomogeneity due to alkaline volatilization in Li-modified (K, Na)NbO_3 lead-free piezoceramics. J Am Ceram Soc 96:2693–2695

[13] Shaw NJ (1989) Densification and coarsening during solid state sintering of ceramics: a review of the models. I. Densification. Powder Metall Intl 2(8):16–21

[14] Rahaman MN (2003) Ceramic processing and Sintering. Marcel Dekker, New York

[15] Zhen Y, Li J-F (2007) Abnormal grain growth and new core–shell structure in (K, Na)NbO_3-based lead-free piezoelectric ceramics. J Am Ceram Soc 90:3496–3502

[16] Patro PK, Kulkarni AR, Harendranath CS (2004) Dielectric and ferroelectric behavior of SBN50 synthesized by solid-state route using different precursors. Ceram Int 30: 1405–1409

[17] Huanosta A, West AR (1987) The electrical properties of ferroelectric $LiTaO_3$ and its solid solutions. J Appl Phys 61:5386

[18] Nobre MAL, Lanfredi S (2001) Phase transition in sodium lithium niobate polycrystal: an overview based on impedance spectroscopy. J Phys Chem Solids 62:1999–2006

[19] Andrew KJ (1999) Dielectric relaxation in solids. J Phys D Appl Phys 32:R57

[20] Shulman HS, Testorf M, Damjanovic D, Setter N (1996) Electrical conductivity, and piezoelectric properties of bismuth titanate. J Am Ceram Soc 79:3124–3128

[21] Wu Y, Cao G (2000) Ferroelectric and dielectric properties of strontium bismuth niobate vanadates. J Mater Res 15:1583–1590

[22] Park BH, Hyun SJ, Bu SD, Noh TW, Lee J, Kim H-D, Kim TH, Jo W (1999) Differences in nature of defects between $SrBi_2Ta_2O_9$ and $Bi_4Ti_3O_{12}$. Appl Phys Lett 74:1907–1909